ELSEVIER

Journal of Fluids and Structures 25 (2009) 26–41

JOURNAL OF FLUIDS AND STRUCTURES

www.elsevier.com/locate/jfs

Nonlinear Krylov acceleration for CFD-based aeroelasticity

Z. Feng[a], A. Soulaïmani[a,*,1], Y. Saad[b,2]

[a]*Department of Mechanical Engineering, École de technologie supérieure, 1100 Notre-Dame Street West, Montreal (QC), Canada H3C 1K3*

[b]*Department of Computer Science and Engineering, University of Minnesota, 4-192 EE/CS Building, 200 Union Street S.E., Minneapolis, MN 55455, USA*

Received 6 October 2006; accepted 6 March 2008
Available online 14 July 2008

Abstract

A nonlinear computational aeroelasticity model based on the Euler equations of compressible flows and the linear elastodynamic equations for structures is developed. The Euler equations are solved on dynamic meshes using the ALE kinematic description. Thus, the mesh constitutes another field governed by pseudo-elastodynamic equations. The three fields are discretized using proper finite element formulations which satisfy the geometric conservation law. A matcher module is incorporated for the purpose of pairing the grids on the fluid–structure interface and for transferring the loads and displacements between the fluid and structure solvers. Two solution strategies (Gauss–Seidel and Schur-complement) for solving the non-linear aeroelastic system are discussed. By using second-order time discretization scheme, we are able to utilize large time steps in the computations. The numerical results on the AGARD 445.6 aeroelastic wing compare well with the experimental results and show that the Schur-complement coupling algorithm is more robust than the Gauss–Seidel algorithm for relatively large oscillation amplitudes.

Keywords: Aeroelasticity; Fluid–structure interaction; Nonlinear coupling; Transonic flow; Gauss–Seidel; Schur-complement; Krylov algorithms

1. Introduction

Multiphysics problems are represented in a wide range of applications. The study of fluid–structure interactions in aerodynamics, the thermo-mechanical coupling problem of turbo-machines and the vibro-aeroacoustic problems are some pertinent engineering examples. Because the solution to these problems requires the coupling of equations from different engineering fields, there is an increase in the computational load and in the complexity of computational procedures. Intensive investigations have been performing on aeroelasticity over the last two decades. A review in this domain can be found in Marshall and Imregun (1996). Transonic airflows around a flexible structure are characterized by the presence of nonlinearities, such as shock waves and flow-induced vibrations (Dowell, 1995). In the classical linear

*Corresponding author. Tel.: +1 5143968977; fax: +1 5143968530.
E-mail addresses: Feng.Zhengkun@etsmtl.ca (Z. Feng), Azzeddine.Soulaimani@etsmtl.ca (A. Soulaïmani), saad@cs.umn.edu (Y. Saad).

[1]Work supported by NSERC and CRIAQ grants.
[2]Work supported by NSF Grant ACI-03055120 and by the Minnesota Supercomputing Institute.

0889-9746/$ - see front matter © 2008 Elsevier Ltd. All rights reserved.
doi:10.1016/j.jfluidstructs.2008.03.006

aeroelasticity theory (Bisplinghoff and Ashley, 1962; Fung, 1969), airflow is assumed to be inviscid and irrotational. Corresponding numerical methods, such as the well-known doublet lattice method (Albano and Rodden, 1969; Rodden et al., 1971), the vortex-lattice method (James, 1972; Kida and Take, 1983; Mook and Nayfeh, 1990), the panel method (Bristow and Hawk, 1982; Johnston et al., 1985; Ojha and Shevare, 1985; Petrie, 1978; Schippers, 1982) and the transonic-small-disturbance (TSD) method (Batina et al., 1988; Goorjian and Guruswamy, 1988; Wissink et al., 1996), can be found in the earlier literature. However, the linear theory cannot accurately predict the transonic dip (Yates et al., 1963), which therefore explains why nonlinear aeroelasticity theories are required. Discussions on the behaviours of the aerodynamic nonlinearity can be found in Bendiksen (2004) and Dowell et al. (2003). The full-potential equation, which describes the nonlinearity of a transonic flow, produces improved solutions when the shock is weak (Shankar and Ide, 1988). However, for flows with strong shocks, a high-order model such as one based on the Euler/Navier–Stokes equations, which provides more complete description of the nonlinearity in transonic regimes, is required to obtain accurate solutions (Bessert and Frederich, 2005; Guruswamy, 1988; Snyder et al., 2003). There is evidently an increase in the computational cost. Although the direct method (Leger et al., 1999), where the fluid and the structural governing equations are combined and treated as a single monolithic system of equations, has advantages on algorithm stability and accuracy, it is impractical to rewrite a completely new code for solving a complex aeroelastic system (Beckert, 2000; Farhat et al., 1998; Farhat and Lesoinne, 2000). In fact, computational aeroelasticity which is characterized by multiphysics is a particular case of fluid–structure interaction (Farhat, 1995). Its evolution is always accompanied by those of the CFD and CSD models which have different mathematical and numerical properties (Farhat and Lesoinne, 2000; Rifai et al., 1999). Fluid dynamics is dominated by the Navier–Stokes/Euler equations while structural dynamics is dominated by the elastodynamics equations. Traditionally, due to the computation complexity and computer technology limitations, a complete aeroelasticity system was analysed using CFD and CSD software separately by different working groups and then using data communication between them. Such loosely coupled strategy becomes less effective for large structures with higher computational accuracy. The coupling strategy in computation replaces the separating working groups through the CSD and CFD solvers with moving mesh and uses an information transfer module for the communication between them (Farhat et al., 1995, 2006). This strategy facilitates the development of the complete software by developing CSD and CFD codes separately. The most interesting feature of this coupling strategy is the reutilization of the existing well-established CSD and CFD codes (Cebral and Lohner, 1997).

In this paper, the aeroelastic system is modelled by three fields (the structural, the fluid and the mesh fields) through an information transfer module. As the focus is on the nonlinear behaviour due to the transonic flow, we assume that the flow is described by the Euler equations and that the structure is modelled through the linear elastodynamic equations rather than nonlinear structural dynamics (Patil and Hodges, 2004). The nonlinear coupling between the structure and the fluid is reinforced by imposing kinematic and dynamic compatibility conditions at the fluid–structure interface (FSI).

One important numerical issue addressed in this paper is to find ways to compute a global solution to the coupled nonlinear fluid–structure problem. There are many possible solutions to the problem. At one extreme one can simply try to solve the whole coupled system by a Newton-type iteration. The disadvantage of this viewpoint is that the various variables of the system do not have the same scale and the meshes for the solid and fluid do not easily match. These can be handled, but the problem will end up being difficult to solve as a whole. At the other extreme, one can simply use a very common ''self-consistent-field'' iteration: solve the fluid problem by fixing the structure variables then update the mesh by using the resulting fluid variables (pressures on the structure), and repeat the process until there is no change in, for example, the structure mesh. This basic procedure can now be accelerated, for example, by a form of nonlinear generalized minimal residual (GMRES). To be specific, we can select one variable to accelerate and proceed to accelerate the fixed-point iteration. There are many choices possible. This paper examines some of these choices and compares them. It is important to note that there are many practical situations in science and engineering which are similar to the one just described. The techniques described in this paper may be applicable to other situations.

The remainder of this work is set out as follows: the governing equations of the complete system are presented, followed by a description of the coupling algorithms and then a discussion of numerical results; we end with concluding remarks.

2. Aeroelasticity problem

Aeroelasticity is one of the most important and challenging examples of multi-physics applications. It couples two nontrivial applications and is characterized by multiscale phenomena, both in time and space. Finding efficient solution to this problem is critically important in the design of aircraft. Coupling between the fluid flow and the flexible structure displacement can produce instabilities which may compromise structural integrity. The flutter is a dynamical instability phenomenon exhibited by a flexible structure under the effect of high flow speed, and so it is thus crucial to ensure that the flexible structure is aeroelastically stable, particularly in the case of structures used as aeronautic components.

2.1. Governing equations

2.1.1. Structure-related equations

The displacement $\mathbf{u}^s$ of a flexible elastic structure satisfies the dynamic equilibrium equations:

$$\rho_s u^s_{i,tt} + \sigma^s_{ij,j}(\mathbf{u}^s) = g_i \text{ in } \Omega_s, \tag{1}$$

where ρ_s is the structure density and $\boldsymbol{\sigma}^{\mathbf{s}}$ is the Cauchy stress tensor. We assume an elastic material of the structure and small structural deformations. Thus, the constitutive relation between the Green strain tensor ε^s and the Cauchy stress tensor reads $\boldsymbol{\sigma}^{\mathbf{s}} = \mathbf{C}^s \cdot \varepsilon^s$, with $\mathbf{C}^s$ being the fourth-order constitutive tensor of the structural material and $\varepsilon^s_{ij,j} = \frac{1}{2}(u^s_{i,j} + u^s_{j,i})$. The structure is subjected to external forces and initial conditions. It is particularly important to ensure that kinematic and dynamic compatibility conditions at the FSI Γ_{fs} are respected.

2.1.2. Fluid-related equations

We assume that the fluid flow is modelled by the compressible Euler equations. These are written in a moving frame of reference, i.e., moving mesh (Donea, 1982; Soulaïmani and Saad, 1998), and in terms of the conservative variables $\mathbf{U} = \rho(1, \mathbf{u}, e + \|\mathbf{u}\|^2/2)^{\mathrm{T}}$ as

$$\mathbf{U}_{,\mathbf{t}} - \mathbf{w}_i \mathbf{U}_{,i} + \mathbf{F}_{i,i} = 0 \text{ in } \Omega_f, \tag{2}$$

where ρ is the fluid density, $\mathbf{u} = \{u_i\}$ is the fluid velocity, p the pressure, e the total energy per unit mass, $\mathbf{F}_i = u_i\mathbf{U} + p(0, \delta_{\mathbf{i}}, u_i)^{\mathrm{T}}$ is the convective flux in the ith direction, $\delta_i = \{\delta_{ij}\}$ is the Kronecker delta and $\mathbf{w} = \{w_i\}$ is the mesh velocity.

2.1.3. Compatibility conditions at the FSI

Since the fluid is assumed to be inviscid, the interface is a *slip* material boundary. That means that we have the following kinematic boundary condition along Γ_{fs}: $(\mathbf{u} - \mathbf{u}^{\mathbf{s}}_{,\mathbf{t}}) \cdot \mathbf{n}^{\mathbf{s}} = 0$ with $\mathbf{n}^{\mathbf{s}}$ being the unit normal vector at Γ_{fs}. The force acting on the structure is due to the fluid pressure. Thus, we have the dynamic compatibility conditions along the interface: $\sigma^s_{ij} n^s_j = -p n^s_i$.

2.1.4. Mesh movement-related equations

The mesh of the fluid domain is animated with its specific motion in order to fulfill the kinematical compatibility constraints (i.e., to preserve material boundary characteristic of the interface) and to maintain the quality of the discretization. This can be done by solving an elliptic problem for the mesh displacement $\mathbf{u}^{\mathbf{m}}$ (Soulaïmani and Saad, 1998). At the FSI the mesh displacement is imposed to that of the structure. To find the displacement of the points in the interior of Ω_f, we assume that the mesh represents an isotropic elastic material and its motion is assumed to be governed by the elastodynamic equations:

$$\rho_m u^m_{i,tt} + \sigma^m_{ij,j}(\mathbf{u}^{\mathbf{m}}) = 0 \text{ in } \Omega_f, \tag{3}$$

where ρ_m is the fictitious mesh density and $\boldsymbol{\sigma}^{\mathbf{m}}$ is the Cauchy stress tensor. The mesh velocity is given by $\mathbf{w} = \mathbf{u}^{\mathbf{m}}_{,t}$. The boundary conditions are: $\mathbf{u}^{\mathbf{m}} = \mathbf{u}^{\mathbf{s}}$ at Γ_{fs} and zero elsewhere. We denote by $\mathbf{F}^m$ the deformation tensor of the mesh movement, i.e., $F^m_{ij} = \delta_{ij} + u^m_{i,j}$. The mesh deformations are not assumed to be small, so the Green strain tensor $\mathbf{E}^m$ is given by $\mathbf{E}^m = \frac{1}{2}(\mathbf{F}^{\mathbf{m}\mathrm{T}}\mathbf{F}^{\mathbf{m}} - \mathbf{I})$. Thus, the constitutive relation between the Green strain tensor $\mathbf{E}^m$ and the second Piola–Kirchoff stress tensor $\mathbf{S}^m$ reads: $\mathbf{S}^m = \mathbf{C}^m\mathbf{E}^m$, with $\mathbf{S}^m = \gamma\, \mathbf{F}^{\mathbf{m}-1}\sigma^m(\mathbf{F}^{\mathbf{m}})^{-\mathrm{T}}$, $\gamma = \det(\mathbf{F}^{\mathbf{m}})$ and $\mathbf{C}^m$ being the fictitious fourth-order tensor for the mesh material.

2.2. Space discretizations

2.2.1. Finite elements for the structure

The equilibrium equations for the structure and for the mesh are discretized using a classical weak variational formulation and finite element interpolations (three-dimensional continuum elements for the mesh, and structural elements such as shells, solids, beams and trusses). The discrete sets of equations for the structure are written in the matrix form as

$$\mathbf{M}^s\{\mathbf{U}^s\}_{,tt} + \mathbf{K}^s\{\mathbf{U}^s\} = \{\mathbf{G}^s(p_{fs})\}, \tag{4}$$

where $\{\mathbf{U}^s\}$ is the set of structural degrees of freedom. Note that by introducing the dynamic boundary conditions at the FSI, the right-hand side of (4) becomes dependent on the fluid pressure. The linear time-dependent system (4) can be

solved either by using a direct time-stepping approach or by using a modal superposition analysis. We adopt the latter approach. Thus, Eq. (4) is transformed into a set of m ordinary differential equations where the unknown is the generalized modal displacement vector $\{\mathbf{Z(t)}\}$:

$$\{\mathbf{Z}\}_{,tt} + \mathbf{\Lambda}\{\mathbf{Z}\} = \{\mathbf{g}^s(p_{fs})\}, \tag{5}$$

where $\mathbf{\Lambda} = \mathrm{diag}(\omega_1^2, \ldots, \omega_m^2)$, ω_i^2 are the m-eigenvalues of the problem: $\mathbf{K}^s\{\phi_i\} = \omega_i^2\mathbf{M}^s\{\phi_i\}$ and ϕ_i are the eigenvectors. The vector of nodal displacements $\{\mathbf{U}^s\}$ is related to $\{\mathbf{Z}\}$ by $\{\mathbf{U}^s\} = \Phi\{\mathbf{Z}\}$ with $\Phi = [\phi_1, \ldots, \phi_m]$ and $\{\mathbf{g}^s\} = \Phi^{\mathrm{T}}\{\mathbf{G}^s\}$.

2.2.2. Finite elements for the fluid

The space discretization of the Euler equations is achieved through the Stream-Line-Petrov-Galerkin method (Hughes and Mallet, 1986; Soulaïmani and Fortin, 1994). Consider a partition of the fluid domain into elements Ω^e. The SUPG formulation reads: find $\mathbf{U}$ such that for all weighting functions $\mathbf{W}$,

$$\sum_e \int_{\Omega^e} (\mathbf{W} + (\mathbf{A}_i^t\mathbf{W}_{,i}) \cdot \tau) \cdot (\mathbf{U}_{,t} - \mathbf{w}_{i,t}\mathbf{U} + \mathbf{F}_{i,i})\, \mathrm{d}\Omega + \sum_e \int_{\Omega^e} v^e \mathbf{W}_{,i}\mathbf{U}_{,j}\, \mathrm{d}\Omega = 0, \tag{6}$$

where $\mathbf{A}_i = \partial F_i/\partial \mathbf{U}$ is the Jacobian matrix of the convective flux, v^e is a positive coefficient dependent on the local residual vector $\mathbf{R} = (\mathbf{U}_{,t} - \mathbf{w}_{i,t}\mathbf{U} + \mathbf{F}_{i,i})$, and the matrix τ is commonly referred to as the matrix of time scales (Hughes and Mallet, 1986; Soulaïmani and Fortin, 1994; Soulaïmani et al., 2001). The SUPG formulation is built as a combination of the standard Galerkin integral form and a perturbation-like integral form depending on the local residual vector. The objective is to reinforce the stability inside the elements. The FE approximation of the variational formulation (6) uses linear piecewise polynomials over tetrahedral elements. The discrete system corresponding to (6) is written as

$$\mathbf{M}^f\{\mathbf{U}^\mathbf{f}\}_{,t} + \mathbf{K}^f(\{\mathbf{U}^f\}, \{\mathbf{W}^f\})\{\mathbf{U}^f\} = \{\mathbf{G}^f\}, \tag{7}$$

where $\{\mathbf{U}^\mathbf{f}\}$ is the set of the fluid nodal degrees of freedom, $\mathbf{M}^f$ is the fluid mass matrix and $\mathbf{K}^f$ is the stiffness matrix of the fluid. Since theses matrices and the right-hand side of (6) are obtained by an integration achieved over a moving domain, they are implicitly dependent on the structural displacement $\{\mathbf{U}^s\}$. Thus, there is a two-way coupling between the structure, the fluid and the moving mesh fields.

2.2.3. Finite elements for the mesh

A standard Galerkin variational formulation is established to solve (3). The corresponding discrete set of equations for the mesh is written in matrix form as

$$\mathbf{M}^m\{\mathbf{U}^m\}_{,tt} + \mathbf{K}^m(\{\mathbf{U}^m\})\{\mathbf{U}^m\} = \{\mathbf{G}^m(\{\mathbf{U}\}^s)\}, \tag{8}$$

where $\{\mathbf{U}^m\}$ is the set of mesh nodal degrees of freedom. Since the density ρ_m can be chosen arbitrarily, we set it to zero. Thus Eq. (8) presents a nonlinear steady problem. To avoid large distortions of small elements as the interface moves, the constitutive material properties of the mesh are chosen in the form $\mathbf{C}^m \simeq \mathbf{I}/|\Omega^e|$, where $|\Omega^e|$ is the volume of the corresponding element. Linear FE approximations over tetrahedral elements are used.

2.3. Time discretizations

Implicit time marching schemes allow the use of large time steps for the structure as well as for the mesh and fluid fields. We adopt the trapezoidal rule (Newmark scheme) to integrate (5). We must solve

$$Z_i^{(n+1)} = \frac{\Delta t^2/4}{1 + \omega_i^2\Delta t^2/4}\left(g^s(p_{fs})^{(n+1)} + \frac{1}{4\Delta t}\left[\frac{Z_i^n}{\Delta t} + \dot{Z}_i^n + \frac{\Delta t}{4}\ddot{Z}_i^n\right]\right), \tag{9}$$

where $\dot{Z}_i^n = 2(Z_i^n - Z_i^{n-1})/\Delta t - \dot{Z}_i^{n-1}$, $\ddot{Z}_i^n = 4(Z_i^n - Z_i^{n-1})/\Delta t^2 - 4\dot{Z}_i^{n-1}/\Delta t - \ddot{Z}_i^{n-1}$, and Δt is the time step.

For the fluid, we choose an implicit scheme where the time derivative is approximated by a second-order backward difference scheme,

$$\{\mathbf{U}^f\}_{,t} \simeq (3\{\mathbf{U}^{\mathbf{f},\mathbf{n}+1}\} - 4\{\mathbf{U}^{\mathbf{f},\mathbf{n}}\} - \{\mathbf{U}^{\mathbf{f},\mathbf{n}-1}\})/(2\Delta t).$$

Inserting this approximation into (7) results in a nonlinear system for the fluid d.o.f. at each time step. The systems of Eqs. (8) and (9) are solved by a Newton-GMRES iterative algorithm (Soulaïmaani et al., 2002).

2.4. Fluid–structure interface

A major stumbling block here lies in the fact that the mesh for the fluid and that for the structure do not match. A mechanism must be incorporated to establish a correspondence from the fluid solver to the structure solver (Fig. 1). Specifically, compatibility conditions must be guaranteed at the interface between the fluid and the structure (Farhat et al., 1998; Lohner et al., 1995; Rifai et al., 1999). Since nodes on both sides of the interface do not need to match, a search algorithm is used to identify the structure element that contains the fluid node. Once this mapping is obtained, local pressure forces are computed at each fluid interface node and then interpolated at the structure interface nodes. The resulting pressure load is used as a boundary condition for the structure. As the structure moves, the displacements of the fluid nodes at the interface are obtained by simple interpolation. These are then used as boundary conditions for the mesh solver. The grid velocity is computed for each fluid node and the kinematic boundary conditions at the interface are updated.

3. Solution methods

The nonlinear aeroelasticity model describing the coupling (Fig. 1) of the fluid, mesh and structure fields can be presented in the following form (Soulaïmani et al., 2005):

$$\begin{Bmatrix} \mathbf{R}_1(\mathbf{Y}, \mathbf{Z}(p_{fs})) \\ \mathbf{R}_2(\mathbf{Y}, \mathbf{Z}(p_{fs})) \end{Bmatrix} = \mathbf{0}, \tag{10}$$

where $\mathbf{Y}$ is the set of fluid and mesh variables which consist of vectors $\mathbf{U}^f$ and $\mathbf{u}^m$, $\mathbf{Z}(p_{fs})$ is the set of structural variables, p_{fs} is the pressure at the FSI, $\mathbf{R}_1$ and $\mathbf{R}_2$ are the nonlinear discrete residuals of the fluid, mesh and structural variables, respectively.

The above coupled system can be formulated as a system of nonlinear equations:

$$F(\mathbf{U}) = 0 \quad \text{with } U = \begin{pmatrix} \mathbf{Y} \\ \mathbf{Z} \end{pmatrix}. \tag{11}$$

There are several approaches for use in solving the system (10) or (11). The first of which involves linearizing the system and using a Newton-type method. The linear system resulting from the linearization would be

$$\mathbf{K}_T \begin{pmatrix} \delta\mathbf{Y} \\ \delta\mathbf{Z}(p_{fs}) \end{pmatrix} = -\begin{pmatrix} \mathbf{R}_1(\mathbf{Y}, \mathbf{Z}(p_{fs})) \\ \mathbf{R}_2(\mathbf{Y}, \mathbf{Z}(p_{fs})) \end{pmatrix}, \tag{12}$$

where $\mathbf{K}_T$ is the tangent matrix, formally written as

$$\mathbf{K}_T = \begin{bmatrix} \mathbf{A} & \mathbf{C} \\ \mathbf{D} & \mathbf{B} \end{bmatrix}. \tag{13}$$

A major difficulty with this "fully coupled" approach is that the coupling sub-matrices $\mathbf{C}$ and $\mathbf{D}$ are not practically available. Indeed, they are difficult to express analytically and their approximation by some approximate differencing formulas would end up being too costly.

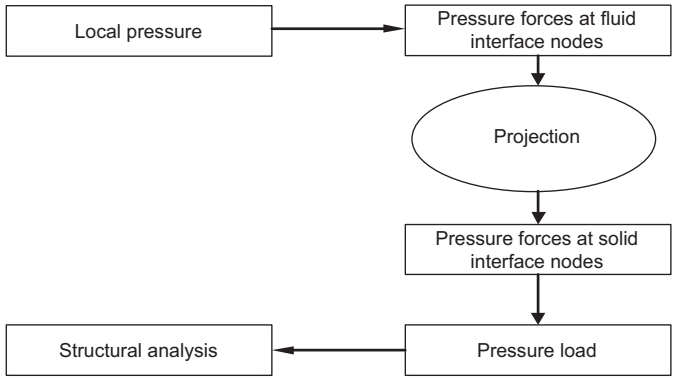

Fig. 1. Fluid–structure data exchange.

An alternative which does not explicitly require Jacobians involves using a nonlinear GMRES procedure to solve the system of nonlinear equations $F(\mathbf{U}) = 0$, [see, e.g., Brown and Saad (1990), Kerkhoven and Saad (1992), Wigton et al. (1985)]. Given the current iterate $\mathbf{U}_n$, we seek a new iterate $\mathbf{U}_{n+1} = \mathbf{U}_n + \delta_n$, where δ_n is in some subspace to be defined shortly. Ideally, we wish to minimize $\|F(\mathbf{U}_n + \delta_n)\|_2$ over this subspace. This is a nonlinear optimization problem which is best solved by using a linear model. Specifically, an approximate solution is obtained by seeking instead to minimize $\|F(\mathbf{U}_n) + J_n\delta_n\|_2$ where J_n is the Jacobian matrix of F at the point $\mathbf{U}_n$. If we were able to exactly solve the linear system $J_n\delta_n = -F(\mathbf{U}_n)$ in the selected subspace, this would just lead to a standard Newton step. A natural idea is to take an *approximate Newton step* which corresponds to selecting the Krylov subspace $K_m = \{v_1, J_n v_1, \ldots, J_n^{m-1} v_1\}$, where $v_1 = -F(\mathbf{U}_n)/\|F(\mathbf{U}_n)\|_2$. This amounts to an inexact Newton iteration where each linear system is approximated by m steps of the (linear) GMRES algorithm. It is also possible to add a backtracking strategy [see, e.g., Brown and Saad (1990)] in order to improve global convergence.

The nonlinear GMRES algorithm is sketched below. The iteration index n is dropped to simplify notation. Note that the algorithm only requires the Jacobian matrix J in the form of matrix-vector products on line 6. Even when the Jacobian is not explicitly available, this product can be performed through a finite difference formula, such as

$$J.v \approx \frac{F(\mathbf{U} + \varepsilon v) - F(\mathbf{U})}{\varepsilon}. \tag{14}$$

Algorithm 1: Nonlinear GMRES

1. **Start:** Choose initial $\mathbf{U}$ and a dimension m of the Krylov subspace.
2. **Arnoldi process**:
3. Compute $\beta = \|F(\mathbf{U})\|_2$
4. and $v_1 = -F(\mathbf{U})/\beta$.
5. For $j = 1, 2, \ldots, m$ do:
6. Compute Jv_j (where J = Jacobian of F at $\mathbf{U}$)
7. $h_{i,j} = (Jv_j, v_i), i = 1, 2, \ldots, j$,
8. $\hat{v}_{j+1} = Jv_j - \sum_{i=1}^{j} h_{i,j} v_i$
9. $h_{j+1,j} = \|\hat{v}_{j+1}\|_2$ and $v_{j+1}\hat{v}_{j+1}/h_{j+1,j}$
10. EndDo
11. Define the $(m+1) \times m$ matrix $\bar{H}_m\{h_{ij}$ if $i \leqslant j+1, 0$ otherwise$\}$
12. and $V_m \equiv [v_1, v_2, \ldots, v_m]$
13. **Form the approximate solution**: Find y_m the minimizer of
14. $\phi(y) \equiv \|\beta e_1 - \bar{H}_m y\|_2$,where $e_1 = [1, 0, \ldots, 0]^T$.
15. Compute $\delta = V_m y_m$
16. **Backtrack**: Choose a damping scalar $\lambda \leqslant 1$ such that
17. $\|F(\mathbf{U} + \lambda\delta)\|_2$ decreases sufficiently relative to $\|F(\mathbf{U})\|_2$.
18. **Restart**: If satisfied stop, else set $\mathbf{U} \leftarrow \mathbf{U} + \lambda\delta$, and goto (2).

Note that this requires one residual evaluation per nonlinear loop (lines 2 to 15) since $F(\mathbf{U})$ does not change throughout this loop and it can be saved.

3.1. Nonlinear block-Jacobi

When the mapping F is linear, i.e, when it is in the form $F(\mathbf{U}) = b - K * \mathbf{U}$, then the algorithm just given would be equivalent to a standard GMRES method for solving the system $K\mathbf{U} = b$, without preconditioning. One preconditioning possibility involves using a block-Jacobi approach which consists of defining the preconditioner as the matrix obtained from neglecting the coupling submatrices C, D in (13):

$$[\mathbf{M}] = \begin{bmatrix} \mathbf{A} & 0 \\ 0 & \mathbf{B} \end{bmatrix}. \tag{15}$$

Unlike the coupling matrices $\mathbf{C}, \mathbf{D}$, the sub-blocks $\mathbf{A}$ and $\mathbf{B}$ are readily available.

Another interpretation of the resulting procedure, is that the nonlinear GMRES algorithm is attempting to accelerate a secant-Newton procedure formed as

$$\begin{pmatrix} \mathbf{Y}_{\text{new}} \\ \mathbf{Z}_{\text{new}} \end{pmatrix} = \begin{pmatrix} \mathbf{Y} \\ \mathbf{Z} \end{pmatrix} - \begin{pmatrix} \mathbf{A}^{-1}\mathbf{R}_1(\mathbf{Y}, \mathbf{Z}(p_{fs})) \\ \mathbf{B}^{-1}\mathbf{R}_2(\mathbf{Y}, \mathbf{Z}(p_{fs})) \end{pmatrix}. \tag{16}$$

The resulting procedure essentially solves Eq. (12) iteratively by replacing the tangent matrix $\mathbf{K}_T$ with the block diagonal matrix (15).

3.2. Nonlinear Gauss–Seidel algorithm

Next, we consider two alternative iterative schemes. The first is a nonlinear Gauss–Seidel iteration whereby the solution of the CFD solver at instant t^{n+1} is computed assuming that the solution of the CSD solver at the same step is already known and *vice versa*, for the solution of the CSD solver. Under well-known conditions (Ortega and Rheinboldt, 1970, Chapter 10) this iteration will be contracting in a certain D, such that it will converge to a unique fixed point for any initial guess in the domain D. At the limit the coupling is 'consistent', in the sense that the pair of solutions found will satisfy both equations at the same time. The overall convergence rate is conditioned by the time step used and by the magnitude of the motion. Though the analysis in Ortega and Rheinboldt (1970) is for the scalar SOR-Newton iteration, it can be generalized to cover a block-SOR case. Recall that the case $\omega = 1$ corresponds to the (Block) Gauss–Seidel iteration. This algorithm is summarized in Algorithm 2.

Algorithm 2: Nonlinear Block Gauss–Seidel iteration

```
1.    Loop over time steps:
2.      Until convergence Do:
3.        Update the fluid field using the new boundary conditions.
4.        Project fluid forces on the structure.
5.        Update the structure displacements.
6.        Update the mesh configuration using the new interface positions.
7.        Check for convergence criterion.
8.      EndDo
9.    EndDo time loop
```

This specific scheme has often been advocated in the literature. For example, in the semi-conductor device simulation literature, it is known as Gummel's method (Kerkhoven and Saad, 1992). Many researchers observed that this form of block-relaxation scheme can be accelerated by a projection-type technique such as GMRES (Brown and Saad, 1990; Wigton et al., 1985; Chan and Jackson, 1984; Reisner et al., 2001). This is based on the observation made above that Algorithm 1 requires the Jacobian only in the form of matrix-vector products which can be evaluated with the simple formula (14). The resulting scheme is often referred to as a nonlinear Krylov method.

The procedure can be described as follows. After each step in Algorithm 2, the iterates undergo a transformation which can be written as

$$\begin{pmatrix} \mathbf{Y}_{\text{new}} \\ \mathbf{Z}_{\text{new}} \end{pmatrix} = \mathbf{M}\begin{pmatrix} \mathbf{Y} \\ \mathbf{Z} \end{pmatrix}, \tag{17}$$

in which M is the nonlinear mapping which corresponds to applying one step of the nonlinear Gauss–Seidel iteration. The iteration is attempting to solve the nonlinear equation:

$$\begin{pmatrix} \mathbf{Y} \\ \mathbf{Z} \end{pmatrix} - \mathbf{M}\begin{pmatrix} \mathbf{Y} \\ \mathbf{Z} \end{pmatrix} = \mathbf{0}. \tag{18}$$

We could consider applying a Newton-like procedure based on Algorithm 1 for solving this system of equations. We will refer to this scheme as a Gauss–Seidel–Newton iteration.

3.3. Nonlinear Schur-complement algorithm

Upon eliminating the $\mathbf{Y}$ variable from system (10), the equations to be solved can be restated in the following form:

$$\mathfrak{R}(\mathbf{Z}(p_{fs}), t) = 0. \tag{19}$$

The idea now is to tackle the above problem as a nonlinear equation in $\mathbf{Z}$. It can be seen that $\mathfrak{R} = \mathbf{R}_2 - DA^{-1}\mathbf{R}_1$. Applying Newton's iteration to Eq. (19), leads to a solution of a linear system of the following form:

$$\mathfrak{R}'(\mathbf{Z})\delta\mathbf{Z} = -\mathfrak{R}(\mathbf{Z}(p_{fs})), \tag{20}$$

where $\mathfrak{R}' = B - DA^{-1}C$ is the Jacobian of $\mathfrak{R}$. Thus, if the problem (19) has a solution, then a solution to the original coupled fluid–structure problem can be easily obtained. When $\delta\mathbf{Z} = 0$, the FSI does not move, which implies that the fluid force does not change. However, the Jacobian $\mathfrak{R}'$ is not practically computable. Since the nonlinear version of GMRES, Algorithm 1, requires only the action of the product of this Jacobian multiplied by a vector $\mathbf{V}$, the matrix $\mathfrak{R}'$ is actually not explicitly needed. Algorithm 1 can be used to solve the Schur-complement problem (19). The products Jv in line 6 of this algorithm can be approximately evaluated by a simple forward finite scheme, analogous to (14):

$$\mathfrak{R}'(\mathbf{Z}) \cdot \mathbf{V} \approx \frac{\mathfrak{R}(\mathbf{Z} + \varepsilon\mathbf{V}) - \mathfrak{R}(\mathbf{Z})}{\varepsilon}, \tag{21}$$

where ε is a small coefficient. The small-size linear system (20) (its size is actually the number of structural dry modes m) converges exactly in m iterations, even without any preconditioning. The most time-consuming part of this algorithm is in the construction of the Krylov subspace. Significant savings can be obtained by freezing the Krylov subspace for a few time-iterations. However, before the Krylov directions can be generated, the pressure at the interface must be determined through the following computational steps.

3.3.1. *Calculation of interface pressures*

1. Compute the coordinates of the structure corresponding to the perturbed modal coordinates $\mathbf{Z} + \varepsilon\mathbf{V}$.
2. Update the coordinates of the fluid nodes at the interface.
3. Update the mesh coordinates.
4. Update the fluid field.
5. Project the fluid pressure on the interface.

4. Numerical results

Numerical simulations were performed on the aeroelastic wing AGARD 445.6. This wing has a symmetrical airfoil NACA 65A004 and a quarter-chord 45° sweepback and is immersed at a zero angle of attack in a transonic airflow. It

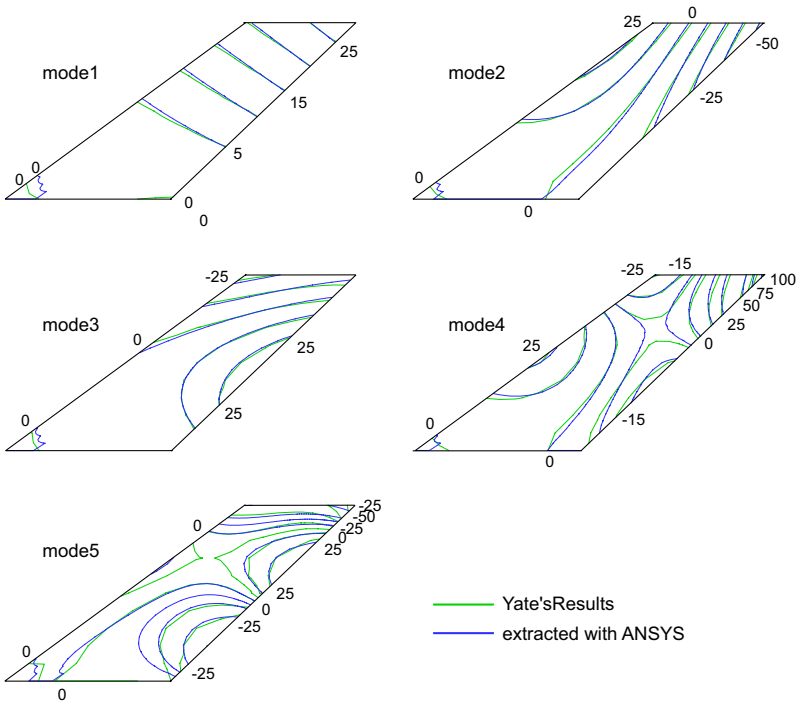

Fig. 2. Modal vectors of wing AGARD 445.6 extracted with ANSYS.

has a mass of 0.1276 slug (1.86227 kg), a Young's modulus of 4.7072×10^5 psi (3.2455×10^9 N/m^2), a Poisson ratio of 0.31 and a density of 0.8088 slug/ft^3 (416.86 kg/m^3). The structural domain is discretized by 1176 quadrilateral shell elements. The modal parameters are extracted using the commercial software ANSYS. The natural frequencies of the first five modes which are 9.6, 39.4, 49.6, 96.1 and 126.3 Hz, and the modal vectors presented in Fig. 2 are in good agreement with the experimental results (Yates et al., 1963). A coarse fluid mesh having 177 042 linear tetrahedral elements and 37 965 nodes is used. Since the strongest variation of the fluid variables occurs around the wing, the elements near the wing are much smaller than those in the rest of the fluid domain. There are 12 921 fluid nodes and 25 684 triangular elements on the wet surface of the wing on which slip boundary conditions are applied. Since the structural motion has no influence on the far-field boundaries, the flow is imposed as the incoming flow. The initial solution for the CFD solver is obtained by considering the wing as a rigid structure. The corresponding fluid configuration is considered as the initial state of the unsteady flow. From this state, a Dirac force is applied on the point located at the intersection between the wing tip and the leading edge. The Mach number of the oncoming flow is chosen as 0.96 in order to simulate the critical point of the transonic dip. The results of the flutter boundary prediction with our parallel code can be found in Soulaïmani et al. (2004).

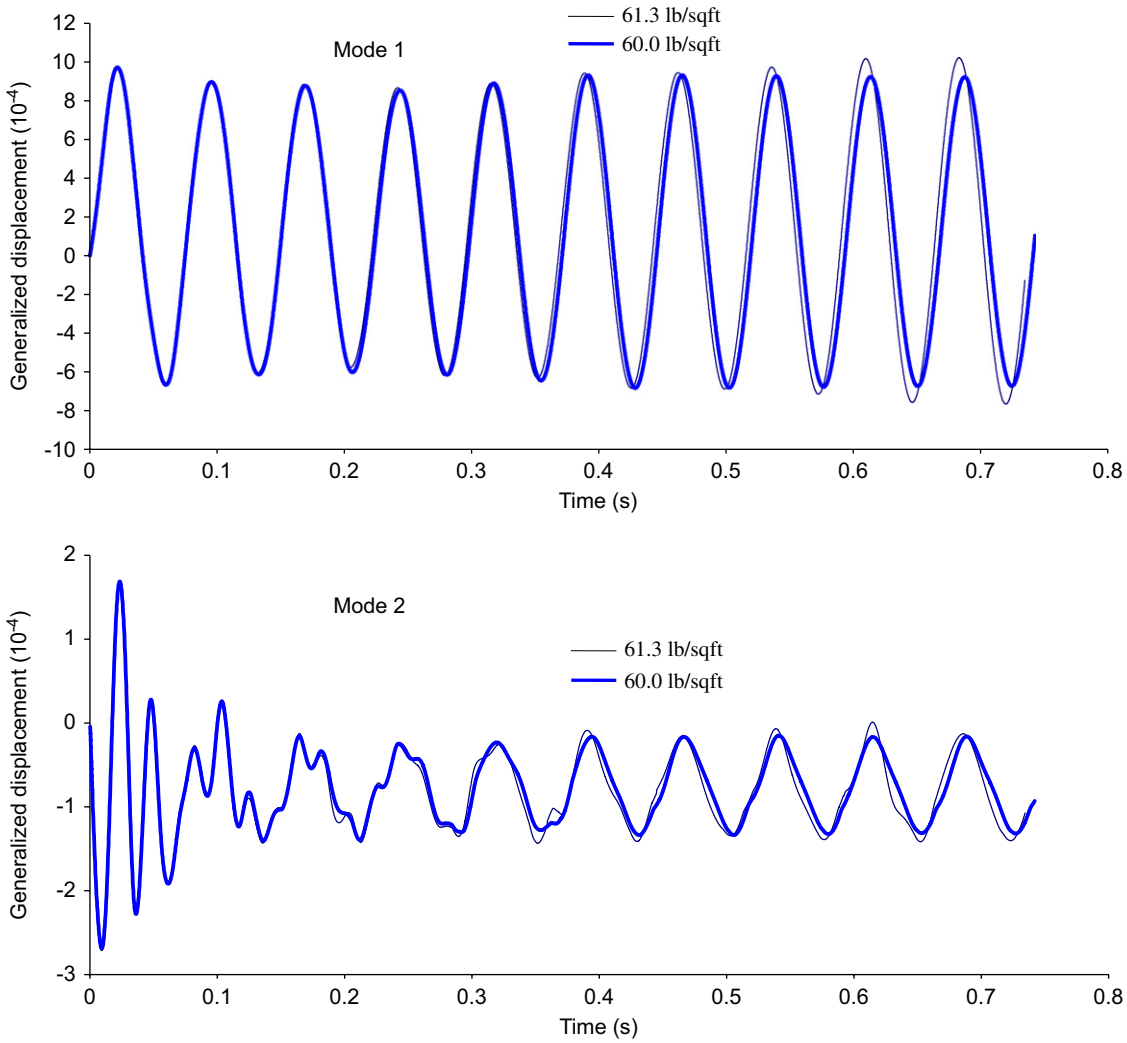

Fig. 3. Time history of the generalized displacements of the first two modes under a load perturbation with nondimensional time step of 0.1 at aerodynamic pressures 60 lb/ft^2 and 61.3 lb/ft^2.

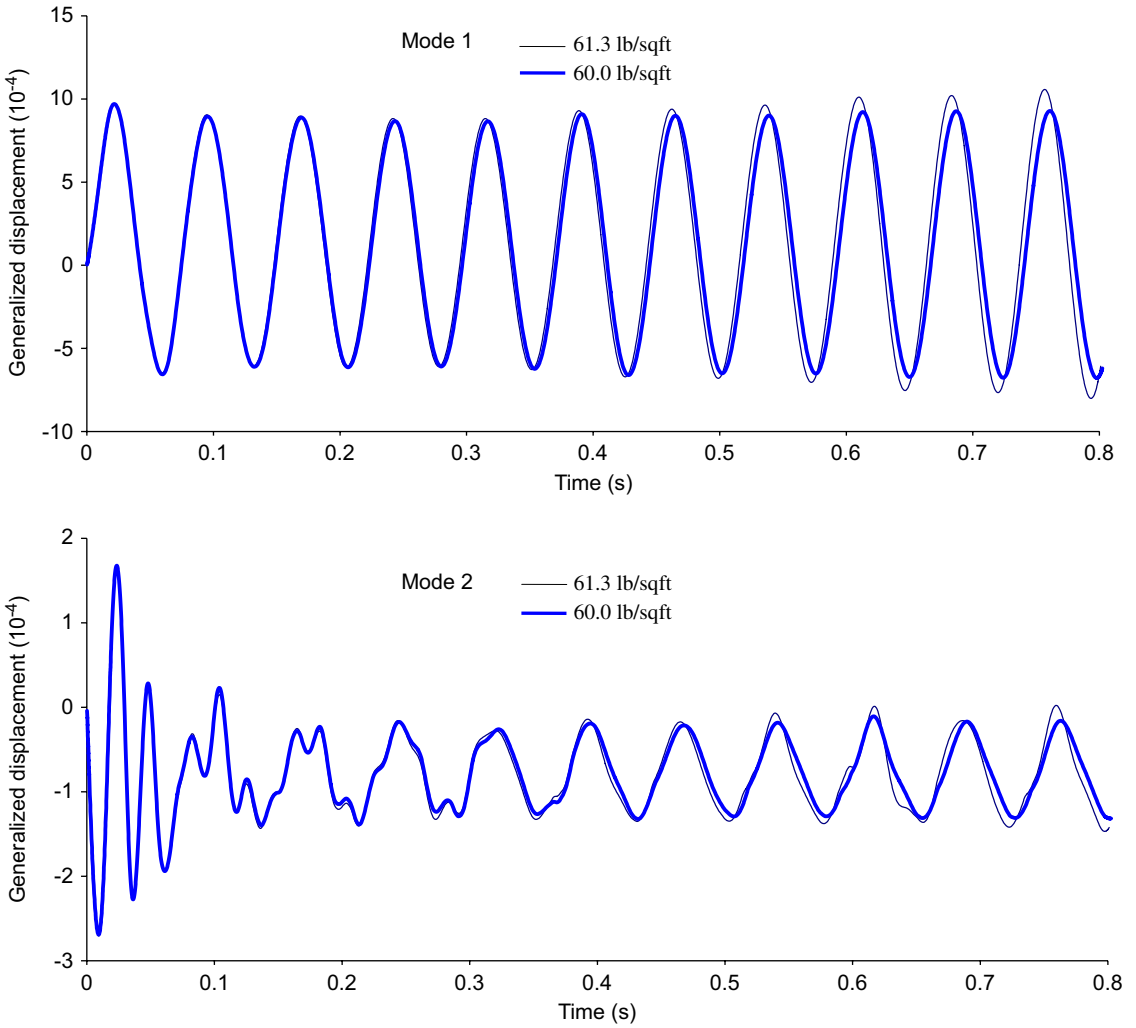

Fig. 4. Time history of the generalized displacements of the first two modes under a load perturbation with nondimensional time step of 0.3 at aerodynamic pressures 60 lb/ft^2 and 61.3 lb/ft^2.

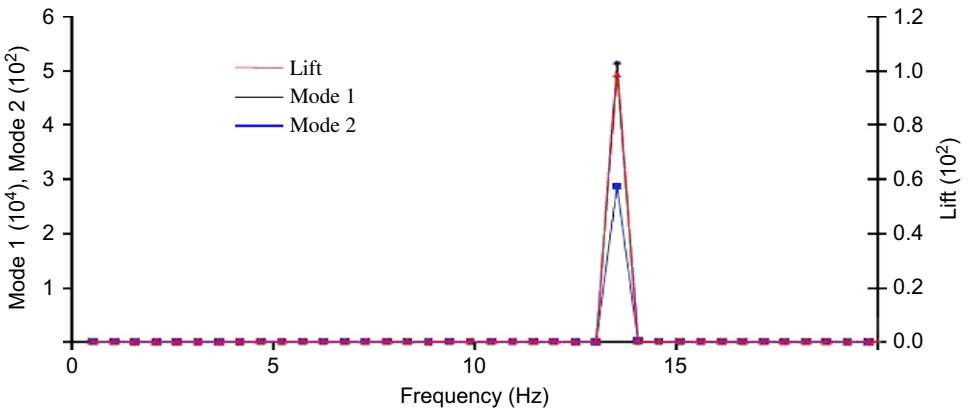

Fig. 5. Spectral distributions of the lift and of the first two modes.

4.1. Numerical simulations with nonlinear Gauss–Seidel coupling algorithm

First, for the purposes of accurately capturing the flutter dip, a relatively small nondimensional time step of 0.1 which corresponds to a real time step of 2.01×10^{-4} s is used in the numerical simulations. At the aerodynamic pressure of $60\,\mathrm{lb/ft^2}$ of the oncoming flow, the amplitudes of the lift and the generalized displacements (z_1, z_2) of the first two modes, which dominate the responses of the structural displacements, are constant and the critical flutter is captured. When the aerodynamic pressure of the oncoming flow increases to $61.3\,\mathrm{lb/ft^2}$, the responses of the amplitudes of the wing increase, and the wing is set beyond the flutter point (Fig. 3). In order to reduce the computing time, the numerical simulations with an increased nondimensional time step of 0.3 are performed, and the flutter point is also captured at the aerodynamic pressure of $60\,\mathrm{lb/ft^2}$. Fig. 4 presents the time histories of the generalized displacement of the first two modes in comparison with another case with a higher aerodynamic pressure of $61.3\,\mathrm{lb/ft^2}$.

At the flutter point with an aerodynamic pressure of $60.0\,\mathrm{lb/ft^2}$ and a Mach number of 0.96, the damping coefficients are very small positives or negatives (see Simulations 1 and 3 in Table 1), the coalesced frequency of 13.5 Hz (84.8 rad/s) of the first two modes is very close to the experimental frequency of 13.9 Hz (87.3 rad/s) (Yates et al., 1963). The spectral distributions of the first two modes obtained with the fast discrete Fourier transform fully confirm the frequency coalescence (Fig. 5). The frequencies of the lift and the first two modes have practically the same value at the flutter point. This flutter aerodynamic pressure also agrees with the computational data in (Gupta, 1996; Lesoinne et al., 2001). When the aerodynamic pressure was increased to $61.3\,\mathrm{lb/ft^2}$, the amplitudes of the generalized displacements of the first two modes start to increase, as does the difference in the frequencies of the oscillation. Table 1 summarizes the damping coefficients and the frequencies of the oscillation of the lift and the generalized displacements of the first two modes of the numerical simulations (Feng, 2005). In Simulations 1 and 3 with an aerodynamic pressure of $60.0\,\mathrm{lb/ft^2}$, the damping coefficients are nearly zero and the frequencies are almost equal. The system reaches the flutter point (Fig. 6). In Simulations 2 and 4 with an aerodynamic pressure of $61.3\,\mathrm{lb/ft^2}$, the damping coefficients become negative, and the difference in the frequencies of the first two modes starts to increase. The responses of the system indicate the flutter (Fig. 7). Simulations 3 and 4 show that the nondimensional time step can be increased from 0.1 to 0.3, and thus the computational speed is almost three times faster than in Simulations 1 and 2.

4.2. Numerical simulations with nonlinear Schur-complement coupling algorithm

The Gauss–Seidel coupling algorithm gives satisfactory results when the perturbation is small. However, it may show signs of numerical instability or may even crash as the perturbation becomes strong. The Schur-complement coupling algorithm can improve the robustness of the code. As the structural displacements increase, the linear mesh model becomes unstable. Fig. 8 shows the comparisons of the generalized displacements of the first two modes obtained by the Schur-complement algorithm with linear and nonlinear mesh models. From this figure, we can see that the code gives the same results at the beginning of the simulations, but the simulation with a linear mesh model stops at one point due to the difficulty of convergence. Fig. 9 shows the comparison of the numerical results obtained from the two nonlinear

Table 1
Frequencies and damping coefficients of the AGARD 445.6 wing

Nondimensional time step	Number of simulation	$p_{ref} = 60\,\mathrm{lb/ft^2}$			$p_{ref} = 61.3\,\mathrm{lb/ft^2}$		
		Simulation 1			Simulation 2		
		Lift	Mode 1	Mode 2	Lift	Mode 1	Mode 2
0.1	Damping	0.00063	0.00063	0.00065	−0.0054	−0.00477	−0.00375
	Frequency (Hz)	13.51	13.53	13.53	13.75	13.6	13.63
	State	Calculated flutter point			Flutter with a small increasing amplitude		
		Simulation 3			Simulation 4		
		Lift	Mode 1	Mode 2	Lift	Mode 1	Mode 2
0.2	Damping	−0.00017	−0.00017	−0.00025	−0.00537	−0.00475	−0.00667
	Frequency (Hz)	13.52	13.52	13.52	13.58	13.58	13.6
	State	Calculated flutter point			Flutter with a small increasing amplitude		

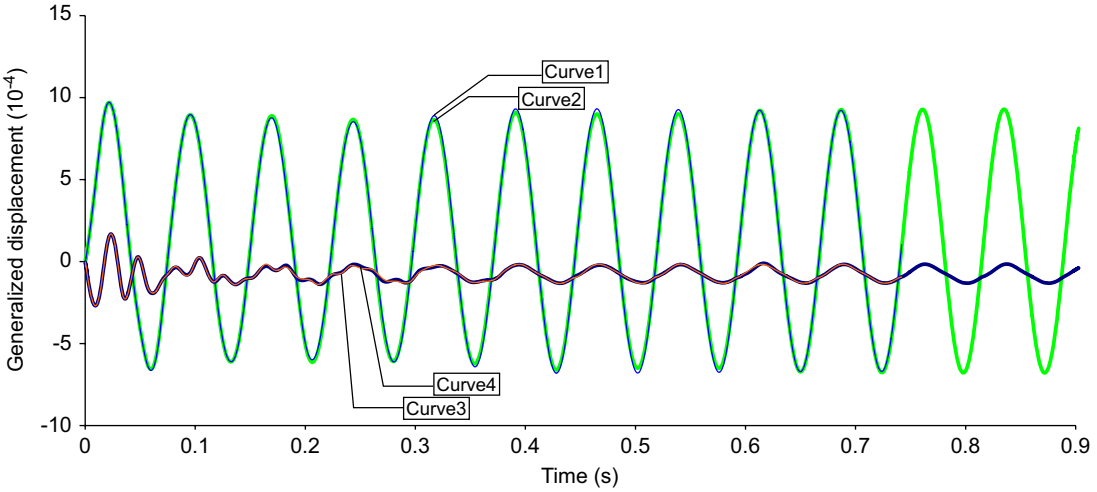

Fig. 6. Time history of the generalized displacements of the first two modes of the wing AGARD 445.6 under a load perturbation with nondimensional time step of 0.1 (curve 1 and curve 3 for mode 1 and mode 2, respectively) and 0.3 (curve 2 and curve 4 for mode 1 and mode 2, respectively); aerodynamic pressure of $q = 60\,\mathrm{lb/ft^2}$.

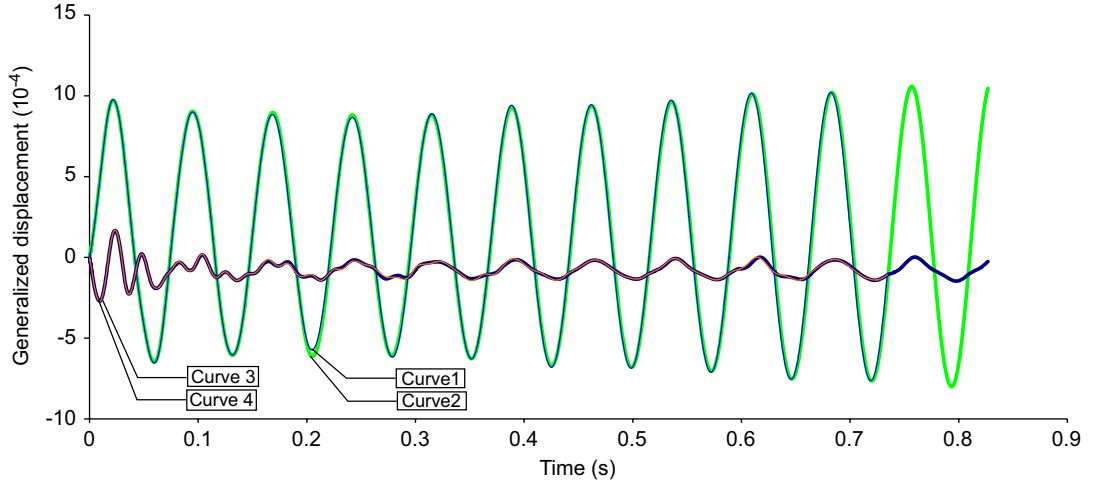

Fig. 7. Time history of the generalized displacements of the first two modes of the wing AGARD 445.6 under a load perturbation with nondimensional time step of 0.1 (curve 1 and curve 3 for mode 1 and mode 2, respectively) and 0.3 (curve 2 and curve 4 for mode 1 and mode 2, respectively), aerodynamic pressure of $q = 61.3\,\mathrm{lb/ft^2}$.

coupling algorithms at a Mach value of 0.96 and an aerodynamic pressure of $60\,\mathrm{lb/ft^2}$. The strong force perturbation yields strong structural displacements which are 20 times larger than that of the test in the previous section. It is observed that the aeroelastic responses with the Schur-complement coupling algorithm are more stable than those with the Gauss–Seidel coupling algorithm.

5. Conclusions

A nonlinear computational aeroelasticity model has been developed using tight coupling algorithms. These coupling techniques re-use the developed linear CSD solver based on the modal analysis and the nonlinear CFD solver modelling the Euler equations. However, a matcher module and a mesh solver are required in order to match the CSD and CFD grids on the fluid–structure interface and to adapt the moving fluid boundaries. Using the second-order time

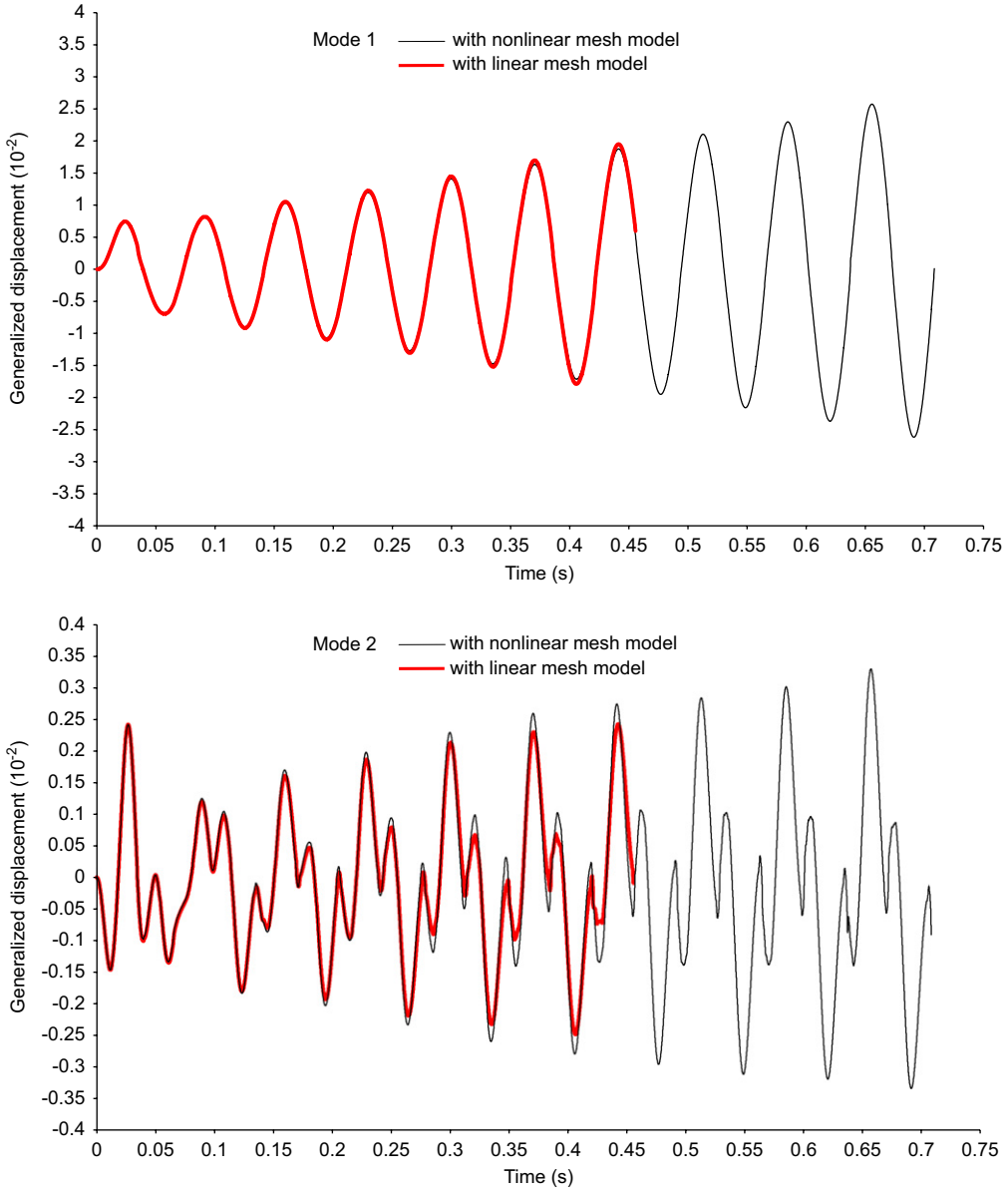

Fig. 8. Comparisons of the generalized displacements obtained by the Schur-complement algorithm with linear and nonlinear mesh models of the first two modes under a load perturbation at aerodynamic pressures 60 lb/ft^2.

discretization scheme and a nonlinear moving mesh model, we are able to use large time steps for the staggered coupling algorithms. This model is applied to the standard aeroelastic wing AGARD 445.6 in order to predict the wing flutter, especially the transonic dip. With a modest perturbation in transonic flows at Mach number 0.96, the results of the flutter simulation by the Gauss–Seidel coupling algorithm agree well with those in the references.

The Schur complement technique proposed in this paper provides a simple, yet effective, solution to the problem of self-consistency in multiphysics simulation. The rationale for this approach is that one can solve for a small set of selected variables in the model. In our case, this set of structural variables corresponds to the number m of modes which is usually small. The reduced system (i.e., Schur complement system), which eliminates the other variables, is then solved by a nonlinear Krylov acceleration. In the linear case, it is possible to show that the method will converge in at most m steps if there are m variables. In our experiments the algorithm converges in m steps despite its nonlinearity. In

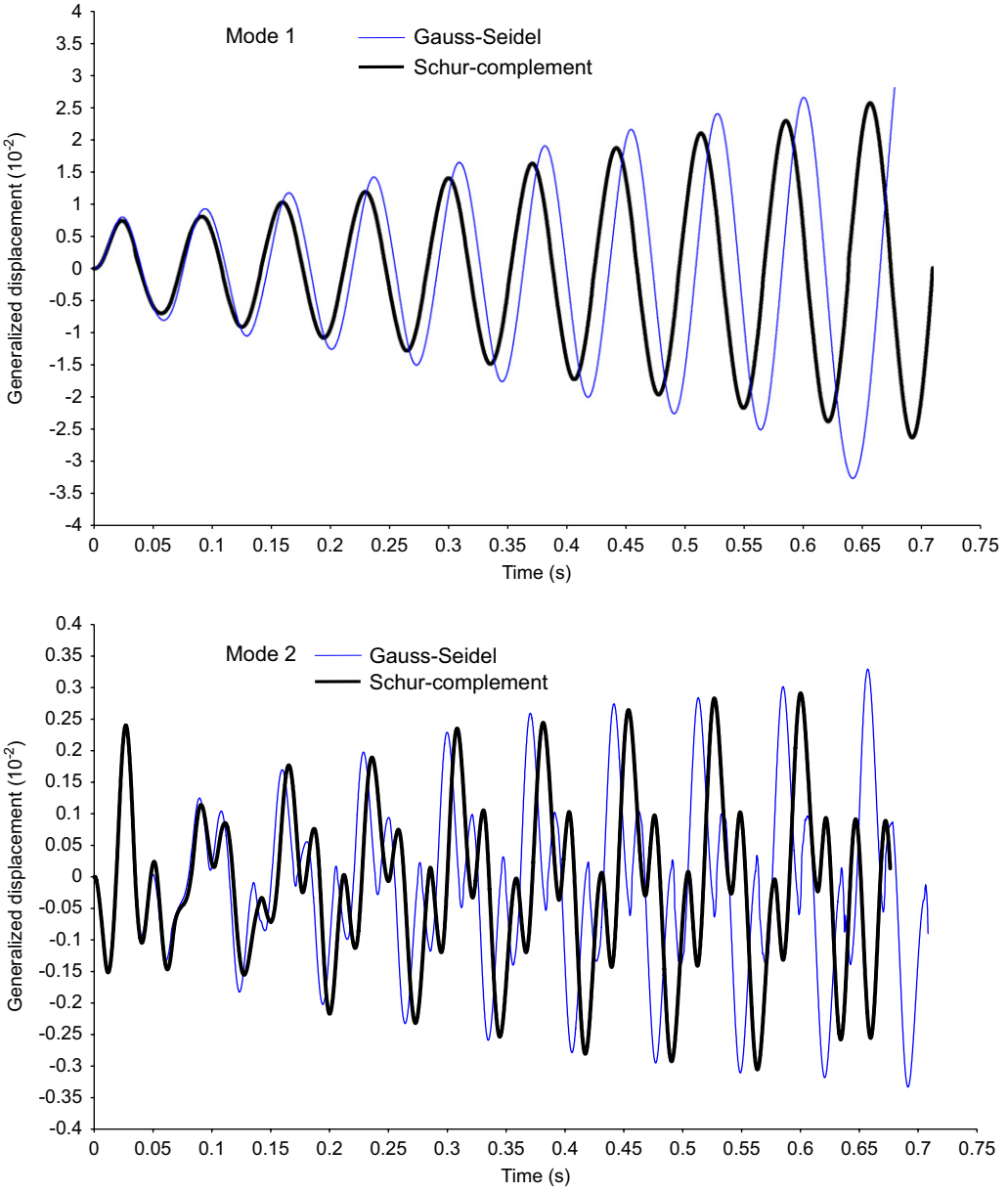

Fig. 9. Comparisons of the generalized displacements obtained by Gauss–Seidel and Schur-complement algorithms of the first two modes under a load perturbation at aerodynamic pressures 60 lb/ft^2.

addition, it appears that under stronger perturbation conditions, this Schur-complement coupling algorithm is more robust than the other approaches with which it was compared.

References

Albano, E., Rodden, W.P., 1969. Doublet-lattice method for calculating lift distributions on oscillating surfaces in subsonic flows. AIAA Journal 7 (2), 279–285.

Batina, J.T., Bennett, R.M., Seidel, D.A., Cunningham, H.J., Bland, S.R., 1988. Recent advances in transonic computational aeroelasticity. Computers and Structures 30 (1–2), 29–37.

Beckert, A., 2000. Coupling fluid (CFD) and structural (FE) models using finite interpolation elements. Aerospace Science and Technology 4 (1), 13–22.

Bendiksen, O.O., 2004. Nonlinear mode interactions and period-tripling flutter in transonic flow. Journal of Fluids and Structures 19, 591–606.

Bessert, N., Frederich, O., 2005. Nonlinear airship aeroelasticity. Journal of Fluids and Structures 21 (8), 731–742.

Bisplinghoff, R.L., Ashley, H., 1962. Principles of Aeroelesticity. Wiley, New York.

Bristow, D.R., Hawk, J.D., 1982. Subsonic panel method for the efficient analysis of multiple geometry perturbations. National Aeronautics and Space Administration (NASA) Contractor Reports.

Brown, P.N., Saad, Y., 1990. Hybrid Krylov methods for nonlinear systems of equations. SIAM Journal on Scientific and Statistical Computing 11, 450–481.

Cebral, J.R., Lohner, R., 1997. Fluid–structure coupling: extensions and improvements. AIAA, Paper 97-0858.

Chan, T.F., Jackson, K.R., 1984. Nonlinearly preconditioned Krylov subspace methods for discrete Newton algorithms. SIAM Journal on Statistical and Scientific Computing 7, 533–542.

Donea, J., 1982. An arbitrary Lagrangian–Eulerian finite element method for transient fluid–structure interactions. Computer Methods in Applied Mechanics and Engineering 33, 689–723.

Dowell, E.H., 1995. A Modern Course in Aeroelasticity, (3rd rev. and enlarged ed). Kluwer Academic Publishers, Dordrecht.

Dowell, E.H., Edwards, J., Strganac, T., 2003. Nonlinear aeroelasticity. Journal of Aircraft 40 (5), 857–874.

Farhat, C., 1995. High performance simulation of coupled nonlinear transient aeroelastic problems. AGARD Report R-807, Special Course on Parallel Computing in CFD, NATO, October 1995.

Farhat, C., Lesoinne, M., 2000. Two efficient staggered algorithms for the serial and parallel solution of three-dimensional nonlinear transient aeroelastic problems. Computer Methods in Applied Mechanics and Engineering 182 (3–4), 499–515.

Farhat, C., Lesoinne, M., Maman, N., 1995. Mixed explicit/implicit time integration of coupled aeroelastic problems: three-field formulation, geometric conservation and distributed solution. International Journal for Numerical Methods in Fluids 21 (10), 807–835.

Farhat, C., Lesoinne, M., Le Tallec, P., 1998. Load and motion transfer algorithms for fluid/structure interaction problems with non-matching discrete interfaces: momentum and energy conservation, optimal discretization and application to aeroelasticity. Computer Methods in Applied Mechanics and Engineering 157 (1–2), 95–114.

Farhat, C., van der Zeeb, K.G., Geuzaine, P., 2006. Provably second-order time-accurate loosely-coupled solution algorithms for transient nonlinear computational aeroelasticity. Computer Methods in Applied Mechanics and Engineering 195 (17–18), 1973–2001.

Feng, Z., 2005. A nonlinear computational aeroelasticity model for aircraft wings. Ph.D. Thesis, École de Technologie Supèrieure, University of Québec, Montreal, Canada.

Fung, Y.C., 1969. An Introduction to the Theory of Aeroelasticity. Dover, New York.

Goorjian, P.M., Guruswamy, G.P., 1988. Transonic unsteady aerodynamic and aeroelastic calculations about airfoils and wings. Computers and Structures 30 (4), 929–936.

Gupta, K.K., 1996. Development of a finite element aeroelastic analysis capability. Journal of Aircraft 33 (5), 995–1002.

Guruswamy, G.P., 1988. Interaction of fluids and structures for aircraft applications. Computers and Structures 30 (1–2), 1–13.

Hughes, T.J.R., Mallet, M., 1986. A new finite element formulation for computational fluid dynamics: III. The generalized streamline operator for multidimensional advective–diffusive systems. Computer Methods in Applied Mechanics and Engineering 58, 305–328.

James, R.M., 1972. On the remarkable accuracy of the vortex lattice method. Computer Methods in Applied Mechanics and Engineering 1 (1), 59–79.

Johnston, C.E., Youngren, H.H., Sikora, J.S., 1985. Engineering applications of an advanced low-order panel method. Paper presented at the Aerospace Technology Conference and Exposition, Long Beach, CA, USA.

Kerkhoven, T., Saad, Y., 1992. Acceleration techniques for decoupling algorithms in semiconductor simulation. Numerische Mathematik 60, 525–548.

Kida, T., Take, T., 1983. A vortex-lattice method in the linear theory on a two-dimensional supercavitating flat plate foil. Computer Methods in Applied Mechanics and Engineering 36 (2), 191–205.

Leger, T.J., Wolff, J.M., Beran, P.S., 1999. Improved determination of aeroelastic stability properties using a direct method. Mathematical and Computer Modelling 30 (11–12), 95–110.

Lesoinne, M., Sarkis, M., Hetmaniuk, U., Farhat, C., 2001. A linearized method for the frequency analysis of three-dimensional fluid/structure interaction problems in all flow regimes. Computer Methods in Applied Mechanics and Engineering 190 (24–25), 3121–3146.

Lohner, R., et al., 1995. Fluid–structure interaction using a loose coupling algorithm and adaptive unstructured grids. AIAA, Paper 95-2259.

Marshall, J.G., Imregun, M., 1996. A review of aeroelasticity methods with emphasis on turbomachinery applications. Journal of Fluids and Structures 10 (3), 237–267.

Mook, D.T., Nayfeh, A.H., 1990. Numerical simulations of dynamic/aerodynamic interactions. Computing Systems in Engineering 1 (2–4), 461–482.

Ojha, S.K., Shevare, G.R., 1985. Exact solution for wind tunnel interference using the panel method. Computers and Fluids 13 (1), 1–14.

Ortega, J.M., Rheinboldt, W.C., 1970. Iterative solution of nonlinear equations in several variables. Academic Press, New York.

Patil, M.J., Hodges, D.H., 2004. On the importance of aerodynamic and structural geometrical nonlinearities in aeroelastic behavior of high-aspect-ratio wings. Journal of Fluids and Structures 19 (7), 905–915.

Petrie, J.A.H., 1978. Surface source and vorticity panel method. Aeronautical Quarterly 29, 251–269.

Reisner, J., Mousseau, V., Knoll, D., 2001. Application of the Newton–Krylov method to geophysical flows. Monthly Weather Review 129, 2404–2415.

Rifai, S.M., Johan, Z., Wang, W.P., Grisval, J.P., Hughes, T.J.R., Ferencz, R., 1999. Multiphysics simulation of flow-induced vibrations and aeroelasticity on parallel computing platforms. Computer Methods in Applied Mechanics and Engineering 174, 393–417.

Rodden, W.P., Giesing, J.P., Kalman, T.P., 1971. New developments and applications of the subsonic doublet-lattice method for nonplanar configurations. In: Symposium on Unsteady Aerodynamics for Aeroelastic in Interfering Surfaces, AGARD CO-80-71, part II, 1971.

Schippers, H., 1982. Application of multigrid methods for integral equations to two problems from fluid dynamics. Journal of Computational Physics 48 (3), 441–461.

Shankar, V., Ide, H., 1988. Aeroelastic computations of flexible configurations. Computers and Structures 30 (1–2), 15–28.

Snyder, R.D., Scott, J.N., Khot, N.S., Beran, P.S., Zweber, J.V., 2003. Predictions of store-induced limit-cycle oscillations using Euler and Navier–Stokes fluid dynamics. Paper presented at the 44th AIAA/ASME/ASCE/AHS/ASC Structures, Structural Dynamics, and Materials Conference, April 7–10, 2003, Norfolk, VA, US.

Soulaïmani, A., Fortin, M., 1994. Finite element solution of compressible viscous flows using conservative variables. Computer Methods in Applied Mechanics and Engineering 118 (3–4), 319–350.

Soulaïmani, A., Saad, Y., 1998. An arbitrary Lagrangian Eulerian finite element formulation for solving three-dimensional free surface flows. Computer Methods in Applied Mechanics and Engineering 162, 79–106.

Soulaïmani, A., Saad, Y., Rebaine, A., 2001. An edge based stabilized finite element method for solving compressible flows: formulation and parallel implementation. Computer Methods in Applied Mechanics and Engineering 190, 5867–5892.

Soulaïmaani, A., Ben Salah, N., Saad, Y., 2002. Enhanced GMRES acceleration techniques for some CFD problems. International Journal of Computational Fluid Dynamics 16, 1–20.

Soulaïmani, A., BenElHajAli, A., Feng, Z., 2004. A parallel-distributed approach for multi-physics problems with application to computational nonlinear aeroelasticity. The Canadian Aeronautics and Space Journal 50 (4), 221–235.

Soulaïmani, A., Feng, Z., Ben Haj Ali, A., 2005. Solution techniques for multi-physics problems with application to computational nonlinear aeroelasticity. Nonlinear Analysis 63 (5–7), 1585–1595.

Wigton, L.B., Yu, D.P., Young, N.J., 1985. GMRES acceleration of computational fluid dynamics codes. In: Proceedings of the 1985 American Institute of Aeronautics and Astronautics (AIAA) Conference, Denver.

Wissink, A.M., Lyrintzis, A.S., Chronopoulos, A.T., 1996. Efficient iterative methods applied to the solution of transonic flows. Journal of Computational Physics 123 (2), 379–393.

Yates, E.C., Land, N.S., Foughner, J.T., 1963. Measure and calculated subsonic and transonic flutter characteristics of a 45° sweptback wing planform in air and in Freon-12 in the Langley transonic dynamic tunnel. National Aeronautics and Space Administration (NASA) Technical Note, D-1616, March 1963.